D. Fátay[a], E. Bastarash[b], K. Nyilas[a], S. Dobatkin[b], J. Gubicza[a,c], T. Ungár[a]

[a] Department of General Physics, Eötvös University, Budapest, Hungary
[b] Moscow State Steel and Alloys Institute, Moscow, Russia
[c] Department of Solid State Physics, Eötvös University, Budapest, Hungary

X-ray diffraction study on the microstructure of an Al–Mg–Sc–Zr alloy deformed by high-pressure torsion

The microstructure and thermal stability of plastically deformed Al-5.9Mg-0.3Sc-0.18Zr alloy have been investigated. Severe plastic deformation has been performed by high-pressure torsion (HPT) straining at room temperature. The microstructure as a function of the number of rotations is studied by X-ray diffraction peak profile analysis. It is concluded that the HPT technique results in a nanostructure with about 40 nm crystallite size. The crystallite size first decreases with the number of rotations, however, after five turns it reaches saturation. The dislocation density increases with turns and the character of the dislocations becomes more edge type. The thermal stability of the nanostructure is studied by differential scanning calorimetry. The stored energy increases with the number of rotations and the maximum of the exothermal peak was shifted to higher temperatures. Increasing the temperature of the the heat treatment, the dislocation density decreases faster than the increase of the mean crystallite size.

Keywords: Al–Mg–Sc–Zr alloy; High-pressure torsion; X-ray peak profile analysis; Crystallite size; Dislocation structure

1. Introduction

Alloying scandium to Al with the appropriate selection of the composition increases the recrystallisation temperature above the solidus [1, 2]. Consequently, the heat treatment during the production of the alloy is not followed by grain growth to preserve the high value of the strength. The increase of the recrystallisation temperature is caused by the formation of coherent Al_3Sc particles at the grain boundaries which hinders the grain boundary motion in the alloy [1, 3]. During long-term heat treatments in the production of the alloys, the grain boundary pinning capability of Al_3Sc particles tends to decrease due to dissolution and corsening of these precipitates [1, 3]. For increasing the thermal stability of Al_3Sc particles, Zr is added to Al alloys together with Sc [1, 2]. The $Al_3(Sc_{1-x}Zr_x)$ phase formed in these alloys preserves all of the positive effect of Al_3Sc mentioned above and acquires new useful properties. Also primary particles of $Al_3(Sc_{1-x}Zr_x)$ are active centers of crystallization of grains of the Al solid solution refining the grain structure of the alloys [1, 4]. During decomposition of the supersaturated solid solution of Al(Sc, Zr), secondary particles of $Al_3(Sc_{1-x}Zr_x)$ are precipitated. These particles cause a strong anti-recrystallization and strenghtening effect with high thermal stability [1, 5, 6].

The need of producing bulk nanostructured alloys leads to the elaboration of severe plastic deformation techniques. In recent years such methods, e. g. high-pressure torsion (HPT), have been widely and successfully used for producing an ultrafine-grained structure in Al alloys [6, 7]. This nanostructure can be retained even at high temperatures with the addition of Sc [8]. The grain size of Al–Sc alloys produced by severe plastic deformation can be further reduced by adding Mg up to 3 % [9]. It was found that the Mg concentration has a strong effect on the superplastic behaviour of these alloys [9].

The analysis of the X-ray diffraction profiles provides information about the size and shape of the diffraction domains (crystallites or grains) and the lattice strains. The classical methods give the apparent size of the crystallites and the mean square strain by the evaluation of the full widths at half maximum, the integral breadth or the first few Fourier coefficients of the peak profiles [10–13]. The development in the computer technique permits the fitting of the whole diffraction profiles by theoretical functions calculated on the basis on the model of the microstructure [14–18]. These procedures can provide the shape and size distribution of the crystallites and parameters characterising the defect structure of the crystal lattice. Beside the size broadening the most well-established peak profile functions have been calculated for dislocations [19, 20]. Using the contrast factors of dislocations, the anisotropic strain broadening of the peak profiles have been rationalized and the dominant dislocation slip system can be determined [21, 22].

Although the effect of the Sc, Zr and Mg additions on the recrystallization resistance and the strength of Al alloys has been extensively studied [e. g. 2, 9], only little information exist on the effect of the extent of severe plastic deformation on the microstructure in Al–Mg–Sc–Zr alloys. In this paper, the formation of the nanostructure in Al-5.9Mg-0.3Sc-0.18Zr alloy (at.%) during HPT was studied by X-ray peak profile analysis. The changes of the crystallite size and the dislocation structure as a function of the deformation are discussed. The thermal stability of the nanostructure is also investigated.

2. Experimental details

The Al-5.9Mg-0.3Sc-0.18Zr alloy (at.%) was deformed by HPT straining. The deformation was performed under 4 GPa pressure on a Bridgman anvil at room temperature. The samples of 15 mm in diameter and 0.6 mm in thickness were deformed by torsion of 0.5, 1, 3, 5, 10 and 15 rotations.

The microstructure of the high-pressure torsion-strained specimens were studied by X-ray diffraction peak profile analysis. The diffraction profiles were measured by a Philips X'pert powder diffractometer using a Cu anode and a pyrolithic graphite secondary monochromator. The step size and the step time were 0.03^0 and 26 seconds/step, respectively. The instrumental corrections were made by using the powder pattern of a Si standard (NBS 640a) and the usual Stokes correction procedure. The first 8 reflections were evaluated by the method of multiple whole profile fitting as it is described in Section 3 of this paper.

The microstructure was also investigated by transmission electron microscopy (TEM) using a JEM–100CX microscope. The average grain size was mesured on bright-field micrographs by the linear intercept method.

The hardness was measured by a Vickers indenter using the load of 0.5 N. The hardness was calculated from the optically measured diagonals of the Vickers pattern.

The thermal stability of the microstructure developed during HPT deformation is studied by differential scanning calorimetry (DSC) using a Perkin-Elmer DSC2 calorimeter. The specimens deformed by 0.5 and 15 rotations were scanned from 320 to 800 K at heating rate of 20 K/min.

3. Evaluation procedure of the X-ray diffraction profiles

The X-ray diffraction peak profiles were evaluated by the multiple whole profile fitting procedure [16, 17]. In this method after the background subtraction and the instrumental corrections, the Fourier transforms of the measured profiles are fitted by the product of the theoretical functions of size and strain broadening. The calculation of the theoretical funtions is based on a model of the microstructure. In this model it is assumed that the crystallites have spherical shape with log-normal size distribution and the lattice strain is caused by dislocations. On the basis of the calculation given in Refs. [17, 18] the Fourier transform of the size profile can be given as:

$$A^S(L) = \frac{1}{2}\mathrm{erfc}\left[\frac{\ln(|L|/m)}{\sqrt{2}\sigma} - 1.5\sqrt{2}\sigma\right] - \frac{1}{4m\exp(2.5\sigma^2)}|L|\mathrm{erfc}\left[\frac{\ln(|L|/m)}{\sqrt{2}\sigma} - \sqrt{2}\sigma\right] + \frac{3}{4m^3\exp(4.5\sigma^2)}|L|^3\mathrm{erfc}\left[\frac{\ln(|L|/m)}{\sqrt{2}\sigma}\right] \quad (1)$$

where L is the Fourier variable, σ is the variance and m is the median of the size distribution function, erfc is the complementary error function. From m and σ the arithmetic, the area- and the volume-weighted mean sizes (diameters) of the crystallites can be determined [23, 24]. In this paper, only the area-weighted mean crystallite size, $<x>_{\mathrm{area}}$, is reported which can be compared with the area-weighted mean grain size obtained from TEM. The area-weighted mean crystallite size can be obtained from σ and m as [23]

$$<x>_{\mathrm{area}} = m\exp(2.5\sigma^2) \quad (2)$$

According to the calculations of Wilkens [20] the distortion (or strain) Fourier coefficients of a peak profile, A^{D}, measured on a dislocated crystal can be expressed as:

$$A^{\mathrm{D}}(L) = \exp[-\rho BL^2 f(\eta)\, g^2\bar{C}] \quad (3)$$

where $B = \pi b^2/2$, b is the absolute value of the Burgers vector, ρ is the dislocation density, $\eta = 1/2[\exp(7/4)]\, L/R_{\mathrm{e}}$, R_{e} is the effective outer cut-off radius of dislocations, g is the absolute value of the diffraction vector, $\bar{C}$ is the average dislocation contrast factor, and $f(\eta)$ is a function derived explicitely by Wilkens (see Eqs. A.6 to A.8 in Ref. [20] and Eqs. (22) and (23) in Ref. [16]). The higher the value of R_e relative to the average distance between the dislocations ($\rho^{-0.5}$), the weaker the dipole character and the screening of the displacement fields of dislocations [20]. In an untextured cubic polycrystalline specimen the values of $\bar{C}$ can be expressed as a function of the indices of reflections, *hkl* [25]

$$\bar{C} = \bar{C}_{h00}\{1 - q(h^2k^2 + h^2l^2 + k^2l^2)/(h^2 + k^2 + l^2)^2\} \quad (4)$$

where $\bar{C}_{h00}$ is the average dislocation contrast factor for the $h00$ reflections and q is a parameter depending on the elastic constants of the crystal and on the character of dislocations (e. g. edge or screw type).

In the multiple whole profile fitting evaluation method first the background is subtracted and the overlapping peaks are separated in one step. In this step of the procedure analytical functions, Voigt, pseudo-Voigt or PearsonVII, plus a linear background are fitted to the overlapping peaks. The functions fitted to the unwanted peaks together with the linear background are subtracted from the measured profile leaving the targeted peak free of the other overlapping peaks and the background. The peaks obtained in this manner are taken as individual diffraction profiles in the evaluation procedure. The Fourier transform of the individual profiles are determined by a non-equidistant sampling Fourier transformation and the experimental Fourier transforms are corrected for instrumental broadening by the Stokes method [26] using a Si standard (NBS 640a). The corrected Fourier transforms are normalised and fitted simultaneously by the products of the theoretical size and strain Fourier transforms given in Eqs. (1) and (3) [16, 17]. The procedure has five fitting parameters for cubic crystals: (i) the median, m, and (ii) the variance, σ, of the log-normal size distribution function, (iii) the dislocation density, ρ, (iv) the outer cut-off radius of dislocations, R_{e} and (v) the q parameter of the dislocation contrast factors characterising the dislocation structure [16, 17].

4. Results and discussion

The X-ray diffraction pattern of the alloy deformed by HPT straining for 0.5 rotation is shown in a logarithmic intensity scale in Fig. 1a. As it can be seen from the figure the main phase is the Al solid solution. The reflections corresponding to this phase are indicated with their indices in the figure. The lattice parameter of the Al solid solution is

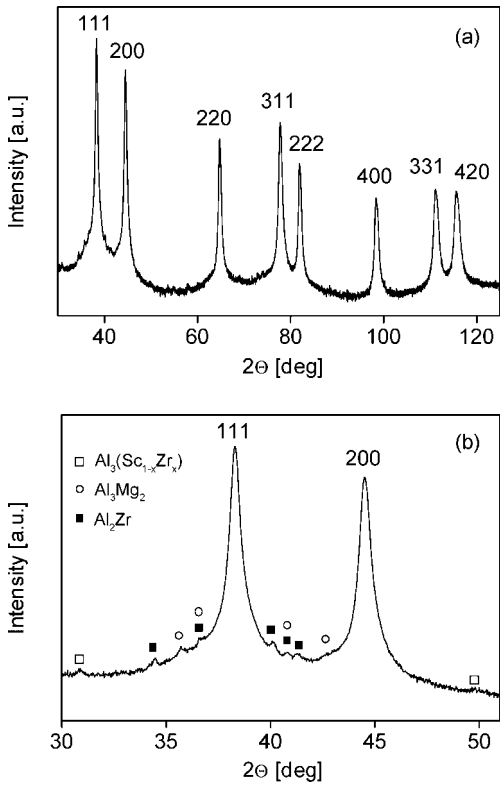

Fig. 1. The X-ray diffraction pattern of the alloy deformed by HPT straining for 0.5 rotation (a). The part of the diffractogram corresponding to 2Θ between 30 and 51° is shown in (b).

0.40721 ± 0.00002 nm which is higher than the value for pure Al: 0.40494 nm. This is probably resulted from the solution of the larger Mg atoms into the Al lattice. Assuming that the increase of the lattice constant is caused only by the Mg solute atoms, the Mg concentration in the solid solution is determined from the Vegard's plot given by Pool and Axon [27]. The Mg concentration is obtained to be 5.38 ± 0.03 at.% which is less than the nominal value of 5.9 at.%. In the tail parts of the 111 and 200 reflections of the Al solid solution, peaks of other minor phases are also observed. For the sake of better visibility, the part of the diffractogram in Fig. 1a corresponding to the diffraction angle 2Θ between 30 and 51° is shown in a wider scale in Fig. 1b. The formation of $Al_3(Sc_{1-x}Zr_x)$ and Al_3Mg_2 in Al–Mg–Sc–Zr alloys has been also observed by Fuller et al. [4]. These phases are most probably formed in the grain boundary, hindering the motion of the grain boundary and consequently increasing the temperature of recrystallisation [4]. The formation of the Mg-rich Al_3Mg_2 phase may be the reason that the measured Mg concentration in Al solid solution is lower than the nominal value. It is noted, however, that the volume fraction of these minor phases estimated from the peak intensities is under 0.3 %. Consequently, these phases are not included in the evaluation of the microstructure and their peaks are subtracted from the profiles of Al as a background. The lattice parameter of the Al solid solution does not change significantly with the increase of the number of rotations while the peaks of the minor phases gradually disappear. Fig. 2 shows the X-ray diffraction pattern of the specimen deformed up to 15 rotations in logarithmic intensity scale. It can be seen that the peaks of the minor phases almost completely disappeared. This may be associated with the fact that one of the main mechanisms

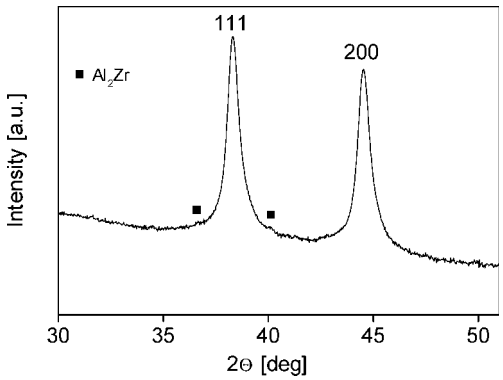

Fig. 2. The part of the X-ray diffraction pattern corresponding to 2Θ between 30 and 51° for the alloy deformed by HPT straining for 15 rotations.

of deformation during severe plastic deformation is grain boundary sliding [9], which could destroy the small grains of the secondary phases, forming thin layers on the grain boundaries of the primary phase. As a consequence of the decay of the grains of the minor phases, the nanostructure probably loses its outstanding resistance to recrystallization at high temperatures.

The measured and the fitted Fourier transforms are shown in Fig. 3a for the specimen subjected to 15 rotations. For a better assessment of the quality of the fitting, the measured (open circles) and fitted (solid lines) Fourier transforms corresponding to the 111, 200 and 220 reflections are shown in a wider scale in Fig. 3b. The difference between the measured and the fitted values is also plotted in the lower parts of the figures with the same scaling as in the main parts of the figures. The agreement between the

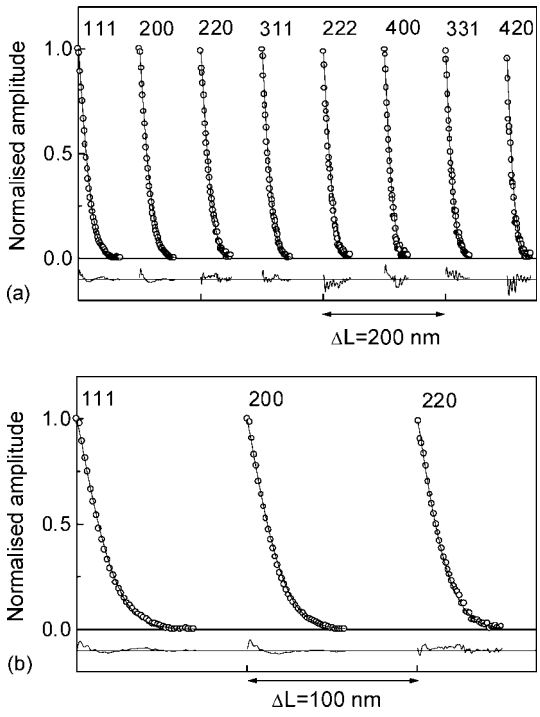

Fig. 3. The measured (open circles) and the fitted (solid line) Fourier transforms for the specimen subjected to 15 rotations (a). The Fourier transforms corresponding to the 111, 200 and 220 reflections are shown in a wider scale in (b). The difference between the measured and the fitted values is also plotted in the lower parts of the figures with the same scaling as in the main parts of the figures.

Table 1. The median, m, and the variance, σ, of the crystallite size distribution, the area-weighted mean crystallite size, $\langle x \rangle_{area}$, the dislocation density, ρ, the outer cut off radius of dislocations, R_e, and the weighted least-squares error, R_{wp}, for different rotations of HPT straining.

Rotations	m [nm]	σ	$\langle x \rangle_{area}$ [nm]	q	ρ [10^{14}m^{-2}]	R_e [nm]	R_{wp} [%]
0.5	39 ± 4	0.36 ± 0.03	54 ± 5	0.64 ± 0.04	16 ± 2	25 ± 2	0.6
1	37 ± 3	0.32 ± 0.02	48 ± 4	0.59 ± 0.04	16 ± 2	26 ± 3	0.8
3	29 ± 3	0.29 ± 0.02	36 ± 4	0.44 ± 0.03	14 ± 2	16 ± 2	0.8
5	26 ± 3	0.37 ± 0.03	37 ± 4	0.46 ± 0.04	24 ± 2	16 ± 2	1.0
10	30 ± 3	0.30 ± 0.02	37 ± 4	0.42 ± 0.03	23 ± 2	13 ± 2	1.0
15	31 ± 3	0.33 ± 0.03	40 ± 4	0.49 ± 0.04	24 ± 2	12 ± 1	1.1

measured and the fitted Fourier transforms is good. The quality of the fitting is characterized quantitatively by the weighted least-squares error (R_{wp}) [28] where the weights are the reciprocal of the observed Fourier transforms. The microstructural parameters obtained from the fitting procedure and the values of R_{wp} are listed in Table 1.

The area-weighted mean crystallite size as a function of the number of rotations is plotted in Fig. 4. It can be established that the HPT straining technique resulted in a nanocrystalline state of the Al–Mg–Sc–Zr alloy with a crystallite size of about 54 nm even after 0.5 rotation. A slight decrease of the size of the crystallites can be observed up to 5 rotations which reaches saturation for further rotations. The dislocation density has a high value even after 0.5 rotation, $16 \cdot 10^{14}$ m^{-2}, and it increases further slightly with the increase of the number of turns. After 5 rotations the dislocation density does not change. The character of dislocations can be obtained from the value of the q parameter. The q parameter values in Al for pure screw and edge dislocations in the $<110>\{111\}$ slip system can be determined by using the detailed numerical calculations and equations in [21] and the elastic constants in [29]. According to this, for pure screw or edge dislocations the values of q are 1.33 or 0.36, respectively. The experimental values of the q parameters obtained for the present HPT-deformed alloys are listed in Table 1 and plotted in Fig. 5 as a function of the rotations. For all the specimens the value of q is lower than the arithmetic mean of the q parameter values corresponding to the pure edge and screw cases. This indicates that the dislocations have more edge character than screw character. A definite tendency of the decrease of the q parameter with the number of rotations can be observed, indicating that the edge character becomes stronger with increasing deformation. The value of the q parameter reaches saturation after 5 turns. The outer cut-off radius of dislocations, R_e, decreases with the number of rotations (see Table 1) which means that the dipole character of the dislocations increases, i. e., the screening of the strain field of adjacent dislocations becomes stronger with the deformation.

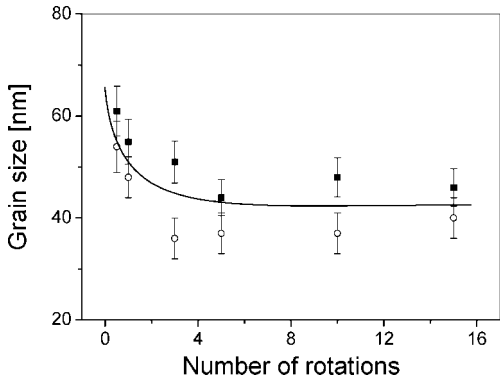

Fig. 4. The area-weighted mean crystallite size obtained from X-ray peak profile analysis (open circle) and the grain size determined by TEM (solid square) as a function of the number of rotations.

Figs. 6 and 7 show TEM micrographs of the alloys deformed by 0.5 and 15 rotations, respectively. The grain size was determined from TEM micrographs for all the specimens and plotted in Fig. 4. It can be established that the values of the crystallite size obtained by X-ray peak profile analysis are somewhat smaller than the grain size determined by TEM. This small difference is not surprising since the number of the grains counted by X-ray analysis is 10^9 times higher than that examined by TEM. The grain size sligthly decreases with the number of rotations up to 5 turns.

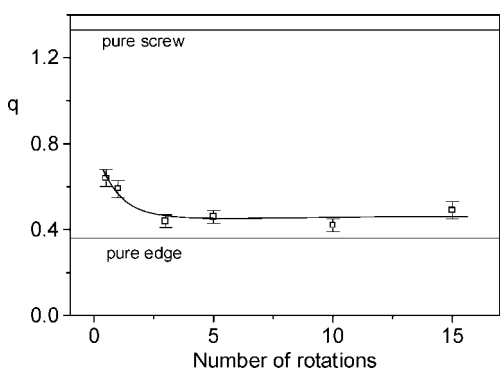

Fig. 5. The q parameter of the dislocation contrast factors as a function of the number of rotations.

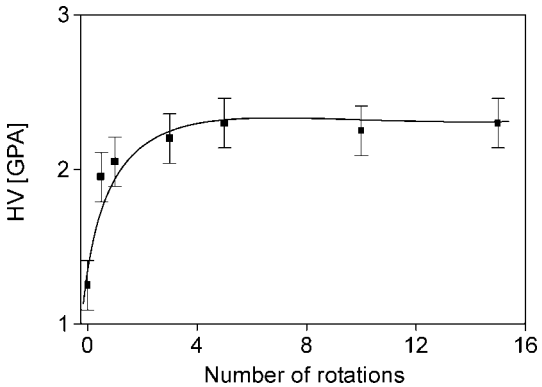

Fig. 6. Bright-field TEM micrograph of the alloy deformed by 0.5 rotation.

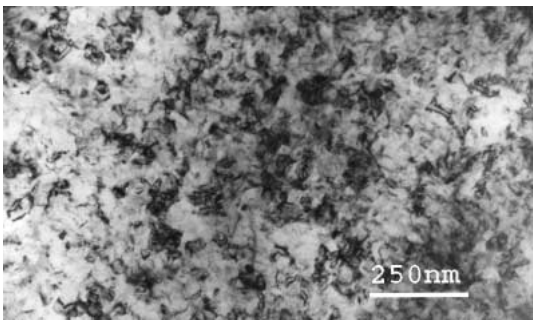

Fig. 7. Bright-field TEM micrograph of the alloy deformed by 15 rotation.

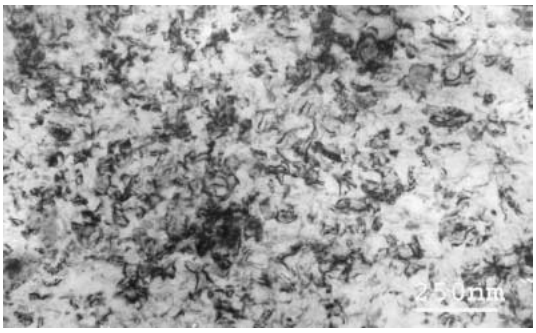

Fig. 8. The Vickers hardness values as a function of the number of rotations.

The values of the Vickers hardness are plotted as a function of the number of rotations in Fig. 8. The hardness increases with the increase of deformation up to 5 rotations due to the increase of the dislocation density and the reduction of the grain size. However, after 5 turns the hardness remains constant since there is no changes in the microstructure if the number of rotations is further increased.

The thermal stability of the microstructure in the specimens deformed by 0.5 and 15 rotations have been studied by DSC between 320 and 800 K. A broad exothermic peak is observed in both DSC curves which corresponds to the release of the stored strain energy during the recovery of the microstructure. These peaks are shown in Fig. 9 where the exothermic heat power normalised to mass unity is plotted as a function of the temperature for the specimens after 0.5 and 15 rotations. It can be seen that the stored energy increases with the increase of deformation and the maximum of the peak is shifted from 450 to 520 K. The increase of the energy released during recovery with increasing rotations can be explained by the increase of the strain and surface energies of the dislocations and the nanosized crystallites, respectively. The temperature of recovery increases probably due to the forming of more stable dislocation structure with dislocation dipoles as it is indicated by the reduction of R_e. To study the recovery of the microstructure, the specimen deformed by 15 rotations was heat-treated in the differential scanning calorimeter up to 450, 520 and 600 K. The mean crystallite size and the dislocation density determined after the heat treatments are listed in Table 2 and plotted as a function of the temperature in Fig. 10. It can be seen that during the recovery of the microstructure, first the dislocation density decreased rapidly by one order of magnitude to $21 \cdot 10^{13}$ m^{-2} while the size of the crystallites remained in the nanometer scale. With further increasing of temperature the crystallite size increased more and more rapidly and it reached 350 nm at 600 K, while the dislocation density reduced to less than 10^{13} m^{-2} which cannot be determined exactly from the peak profiles; therefore, it is taken to be practically zero in Fig. 10.

Table 2. The area-weighted mean crystallite size, $\langle x \rangle_{area}$ and the dislocation density, ρ, of the alloy deformed under 15 rotations after the heat treatment at different temperatures. At 600 K the dislocation density falls under 10^{13} m^{-2}, consequently the exact its value can not be determined from the peak profiles.

T [K]	$\langle x \rangle_{area}$ [nm]	ρ [10^{13} m^{-2}]
300	40 ± 4	240 ± 20
450	60 ± 5	21 ± 3
520	98 ± 6	3 ± 1
600	350 ± 30	–

5. Conclusions

The microstructure produced by HPT straining in Al-5.9Mg-0.3Sc-0.18Zr alloy was studied by X-ray peak profile analysis. It can be concluded that the HPT deformation gives a very fine microstructure after a few rotations, preserving the secondary grain boundary phases which are important for the thermal stability of the nanostructure.

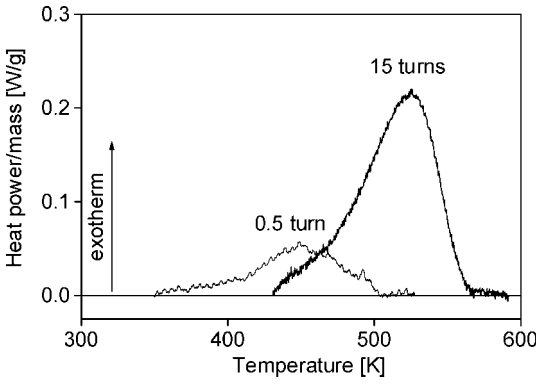

Fig. 9. The DSC curves normalised to the sample mass after the subtraction of the baseline for the specimens deformed by 0.5 and 15 rotations.

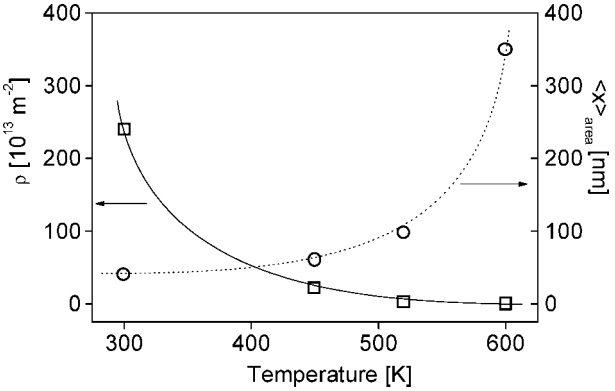

Fig. 10. The area-weighted mean crystallite size and the dislocation density of the specimen deformed by 15 rotations as a function of the temperature of heat treatment.

However, after about 5 turns there is no further refinement in the microstructure, but the grain boundary phases are destroyed, resulting in the loss of the excellent resistance against recrystallization.The recovery of the microstructure occurs between 450 and 520 K which is accompanied by the release of the stored energy. During the recovery first the dislocation density decreases and the crystallite size starts to increase only when the majority of the dislocations is annihilated.

This work was supported by the Hungarian Scientific Research Fund, OTKA, Grant Nos. T031786, T034666 and T029701. J. G. is grateful for the financial support of Magyary Zoltán postdoctoral program of Foundation for Hungarian Higher Education and Research (AMFK). The authors greatly thank Prof. V. V. Zakharov and Dr. T. D. Rostova who kindly presented the Al–Mg–Sc–Zr alloy.

References

[1] V.G. Davydov, T.D. Rostova, V.V. Zakharov, Yu.A. Filatov, V.I. Yelagin: Mat. Sci. Eng. A 280 (2000) 30.
[2] V. Ocenasek, M. Slamova: Mat. Charact. 47 (2001) 157.
[3] E.A. Marquis, D.N. Seidman: Acta mater. 49 (2001) 1909.
[4] C.B. Fuller, A. R. Krause, D.C. Dunand, D.N. Seidman: Mat. Sci. Eng. A (2002), in press.
[5] V.I. Ealgin, V.V. Yakharov, T.D. Rostova: Metallov. i Termicheskaya Obrabotka Metallov No. 1 (1992) 24.
[6] V.V. Stolarov, V.V. Latysh, V.A. Shundalov, D.A. Salimonenko, R.K. Islamgaliev, R.Z. Valiev: Mat. Sci. Eng. A 234–236 (1997) 339.
[7] I.V. Alexandrov, R.Z. Valiev: Scripta mater. 44 (2001) 1605.
[8] S.V. Dobatkin, V.V. Zakharov, R.Z. Valiev, in: G. Gottstein, D.A. Molodov (Eds.), Proc. First Joint Int. Conf. on Recrystallization and Grain Growth, Springer-Verlag, Berlin (2001) 509.
[9] M. Furukawa, A. Utsunomiya, K. Matsubara, Z. Horita, T.G. Langdon: Acta mater. 49 (2001) 3829.
[10] G.K. Williamson, W.H. Hall: Acta metall. 1 (1953) 22.
[11] B.E. Warren, B.L. Averbach: J. Appl. Phys. 21 (1950) 595.
[12] B.E. Warren: Progr. Metal Phys. 8 (1959) 147.
[13] T. Ungár, A. Borbély: Appl. Phys. Lett. 69 (1996) 3173.
[14] P. Scardi, M. Leoni, Y.H. Dong: Eur. Phys. J. B 18 (2000) 23.
[15] P. Scardi, M. Leoni: Acta Cryst. A 58 (2002) 190.
[16] T. Ungár, J. Gubicza, G. Ribárik, A. Borbély: J. Appl. Cryst. 34 (2001) 298.
[17] G. Ribárik, T. Ungár, J. Gubicza: J. Appl. Cryst. 34 (2001) 669.
[18] T. Ungár, J. Gubicza, G. Ribárik, C. Pantea, T.W. Zerda: Carbon 40 (2002) 929.
[19] M. Wilkens: Phys. Stat. Sol. (a) 2 (1970) 359.
[20] M. Wilkens, in: J.A. Simmons, R. de Wit, R. Bullough (Eds.), Fundamental Aspects of Dislocation Theory, Vol. II, Nat. Bur. Stand. (US), Spec. Publ. No. 317, Washington, DC (1970) 1195.
[21] T. Ungár, I. Dragomir, Á. Révész, A. Borbély: J. Appl. Cryst. 32 (1999) 992.
[22] I.C. Dragomir, T. Ungár: J. Appl. Cryst. 35 (2002) 556.
[23] W.C. Hinds: Aerosol Technology: Properties, Behavior and Measurement of Airbone Particles, Wiley, New York (1982).
[24] J.I. Langford, D. Louer; P. Scardi: J. Appl. Cryst. 33 (2000) 964.
[25] T. Ungár, G. Tichy: Phys. Stat. Sol. (a) 171 (1999) 425.
[26] R. Stokes: Proc. Phys. Soc. London 61 (1948) 382.
[27] D.M. Pool, H.J. Axon: J. Inst. Met. 80 (1952) 599.
[28] D. Balzar: J. Res. Nat. Inst. Stand. Technol. 98 (1993) 321.
[29] R.F.S. Hearmon, in: K.-H. Hellwege, A.M. Hellwege (Eds.), Landolt-Börnstein, Springer-Verlag, Berlin (1984) 1.

(Received December 16, 2002)

Correspondence address

Prof. Tamas Ungár
Department of General Physics
Eotvos University
Budapest, P. O. Box 32, H-1518, Hungary
Tel.: +36 1 372 2801
Fax: +36 1 372 2811
E-mail: ungar@ludens.elte.hu